www.elsevier.com/locate/memsci

Regulating the aqueous phase monomer balance for flux improvement in polyamide thin film composite membranes

D.H.N. Perera, Q. Song, H.A.M. Qiblawey, E. Sivaniah

PII: S0376-7388(15)00216-1
DOI: http://dx.doi.org/10.1016/j.memsci.2015.03.038
Reference: MEMSCI13549

To appear in: *Journal of Membrane Science*

Received date: 10 November 2014
Revised date: 17 February 2015
Accepted date: 14 March 2015

Cite this article as: D.H.N. Perera, Q. Song, H.A.M. Qiblawey, E. Sivaniah, Regulating the aqueous phase monomer balance for flux improvement in polyamide thin film composite membranes, *Journal of Membrane Science*, http://dx.doi.org/10.1016/j.memsci.2015.03.038

Regulating the aqueous phase monomer balance for flux improvement in polyamide thin film composite membranes

D.H. N. Perera [a], Q.Song [a], H.A.M. Qiblawey [c] and E. Sivaniah* [a,b]

[a] Cavendish Laboratory, Department of Physics, University of Cambridge, J J Thomson Avenue, Cambridge, CB3 0HE, UK

[b] Institute for Integrated Cell-Material Sciences (iCeMS), Kyoto University

[c] Department of Chemical Engineering, College of Engineering, Qatar University

4/3/2015

* Corresponding Author: Dr. Easan Sivaniah

esivaniah@icems.kyoto-u.ac.jp, es10009@cam.ac.uk;

Tel: 0081 75 753 9744

Keywords: Reverse Osmosis, Desalination, Interfacial Polymerization.

Abstract

Polyamide thin film composite (PA TFC) membranes are synthesized from interfacial polymerization using two amines in the aqueous phase. The conventional monomer, m-phenelynediamine (MPD), is partially replaced by a linear monomer, 1,3–diamino-2-hydroxypropane (DAHP). The water permeability of the membranes improves by around 22 % (to 2.67 ± 0.09 $L.m^{-2}.h^{-1}.bar^{-1}$) while keeping the same high salt rejection (96-98%) at an optimum DAHP/MPD ratio of 12.8 %. While developing the control PA TFC membrane we introduce a washing step and show that the support surface should be free from surface protective coatings to achieve high water flux (2.18 ± 0.08 $L.m^{-2}.h^{-1}.bar^{-1}$). Incorporating DAHP units into the polyamide network improves the water flux through the membranes fabricated on both original and washed supports. The surface morphologies of polyamide films change significantly with introduction of DAHP, from large ridge-and-valley structure to enlarged nodular structures. High resolution SEM images show an ultrathin polyamide thin film with a thickness that is reduced with addition of DAHP. These influences of DAHP, namely a reduction in the selective layer thickness, an alteration in surface morphology, changes in internal molecular packing and hydrophilicity, are suggested as factors behind the improved water permeability.

1. Introduction

In the shadows of drastic environmental changes and ever-increasing population, desalination remains the promising solution to affordable clean water for many nations. Industrially proven state-of-the-art reverse osmosis (RO) desalination membranes have been dominated by polyamide thin film composite (PA TFC) membranes[1]. Therefore it remains important to understand the structural-property relationship of polyamide membranes. .

Commercial polyamide membranes are synthesized from polymerization of 1,3,5-benzenetricarbonyl trichloride (TMC) and m-phenylenediamine (MPD) at the interface of the organic (TMC) and aqueous (MPD) precursor phases. The reaction pathway is illustrated in Figure 1(a). The polyamide thin film layer, consists of two main regions: (i) a thin and highly cross linked primary layer made by interfacial diffusion of the aqueous phase monomer into the organic phase and (ii) a rough secondary layer consisting of the ridge-and-valley structure and nodules which is formed from an aqueous phase diffused through the primary layer [2–4]. The chemical structure and physical properties of these two layers are of significant importance to both water flux and salt rejection. These properties can be tailored by controlling the diffusion rates of the monomers [2,3,5]. The high water flux through PA TFC membrane is believed to be a result of the ultra-thin selective layer and the ridge-and-valley surface structure, which creates a high area at the membrane-water interface [6,7].

The performance of PA membranes in RO process in terms of water flux and salt rejection can also be tailored by increasing the reactivity between the two monomers with catalysts such as camphor sulfonic acid and triethylamine [7–9]. The polymer's carboxylic acid density and the chain packing density [4,10–12] also might affect the water flux and salt rejection. The density of

carboxylic acid groups can be improved by accelerating the hydrolysis of organic phase monomer using additives [13,14] and by introduction of hydrophilic groups such as sulfonic acid or carboxylic acid to the monomers [15–17]. The tuning of packing density and the reaction kinetics remain complex but can be controlled by the structure of monomers. For example, Li *et al.* [18] replaced the conventional organic phase monomer with a bulky and rigid acyl chloride containing two aromatic rings, and found that the flux is reduced with an increase in the salt rejection. This was attributed to the increased chain stiffness and cross-linking density. Wang *et al.* introduced a triamine into the aqueous phase and observed that the water flux improved in the presence of the bulky triamine but with a slight reduction in the salt rejection [17]. The structure-performance relationship therefore remains complex to understand. It should also be noted that most of the studies related to different monomer structures pay less attention to the mechanism of membrane formation. When these monomers are used for polymerization, the reaction kinetics would be different making it difficult to understand the mechanism *via* direct comparison.

In this paper, we report a hydrophilic aliphatic monomer (1,3–diamino-2-hydroxypropane, DAHP) as a partial replacer for the conventional aromatic monomer (m-phenylenediamine, MPD). As shown in Figure 1(a), the DAHP unit can be incorporated into the polyamide network. The molecular structures of polymer segments are determined with molecular simulation software, as shown in Figure 1(b-e). Aliphatic units are assumed to introduce flexibility to the rigid aromatic polymer structure for improved chain mobility that can support water transportation. The hydroxyl group is expected to add additional hydrophilicity to the polymer network. Here we assume that the hydroxyl groups in DAHP can be maintained to some extent though it can also react with the chloride groups in TMC to form ester linkages. We show that partial substitution of DAHP monomers effectively improves the water flux while keeping the

same high salt rejection. We discuss the observed changes of desalination performance and the possible formation mechanism of polyamide thin films. We show that by controlling the balance of linear-aromatic monomers and the hydrophilicity of the aqueous phase monomers, but without hindering the monomer equilibrium, the performance of PA TFC membrane can be improved. This is in contrast to another report which has used the same monomer as an additive and in high percentage where the reactant balance was neglected and thus the membrane performance was deteriorated [19]. While developing the control membrane, we also show that a polysulfone support free from surface coatings is very important for PA TFC membranes with high flux.

2. Experimental details.

2.1 Materials. Polysulfone support (PS20, molecular weight cut-off 20K) was purchased from ATRWater (ROCHEM UF-Systeme GmbH, Germany) and used with or without a pre-washing treatment. 1,3,5-benzenetricarbonyl trichloride (TMC, 98 %), m-phenylenediamine (MPD, ≥ 99 %), 1,3–diamino-2-hydroxypropane (DAHP, ≥ 98%), dodecane (anhydrous, ≥ 99 %), hexane (anhydrous,≥ 99 %), sodium carbonate (anhydrous, ≥ 99 %) and ethanol (96%) were purchased from Sigma-Aldrich and used as received.

2.2 Preparation of PA and PA-DAHP TFC membranes. Polysulfone supports were used as received, or after washing in 70 % ethanol for 1 h followed by rinsing with pure water for 10 min. The washing was done on an orbital shaker (Grant PSU-10i, Grant Instruments) at 120 rpm at room temperature. The washed supports were stored in water until use and the surface was thoroughly dried before contacting with MPD. PA thin films were synthesized on these polysulfone supports by interfacial polymerization following an optimized method described by Xie *et al.* [7]. In brief, the support was fixed onto a frame and immersed in a 1.5 (w/v) % MPD

(aq) solution for 10 min. For the PA-DAHP membranes, DAHP monomer at different concentrations were introduced into the aqueous solution to partially replace the MPD. After removing excess MPD with tissue, a squeeze roller was used to dry the surface-adhered water layer. Next, the support was mounted onto a frame and gasket unit, 0.05 (w/v) % TMC in dodecane solution was poured onto the surface and kept in contact for 1 min. After removing excess TMC, the membrane was washed with hexane, air dried for 1 min and washed in 0.2 % sodium carbonate (aq) solution for 10 min, followed by washing in distilled water for another 15 min. The membranes were stored in distilled water overnight and tested in a dead-end filtration system.

2.3 Characterization of Membranes

Atomic Force Microscopy (AFM). PA TFC membranes were mounted onto Si wafer using double-sided tape and surface profiles were measured using Nanosurf AFM (Nanosurf AG, Switzerland) with tapping mode. The data was analyzed using a scanning probe microscopy data analysis and visualization software Gwyddion (Department of Nanometrology, Czech Metrology Institute). The root mean square roughness is considered as surface roughness and was directly calculated from the software.

Attenuated Total Reflectance Infrared Spectroscopy (ATR-FTIR). Polysulfone supports and PA TFC membranes were dried in silica gel overnight and the active surface was analyzed with ATR-FTIR (Bruker Tensor 27, Bruker) with a diamond crystal and at a 45° incident angle over a range of 525 cm^{-1} – 4000 cm^{-1}. The data were analyzed using the statistical software Igor Pro6 (WaveMetrics Inc., USA).

Contact Angle Measurements: The static water contact angle was determined by the sessile drop method [20] using a KSV CAM 200 goniometer (KSV Instruments) with deionized water. In brief, a droplet of 3 µl of deionized water was placed onto a dry membrane surface, and a static image of the droplet in equilibration with the membrane surface was taken. Image analysis and contact angle computation were performed using the CAM2008 software. At least ten measurements were taken on different place of each PA TFC membrane.

Scanning Electron Microscopy (SEM). PA TFC membranes were freeze-fractured, gold coated and observed using a S5500 SEM (Hitachi) at 5 keV. Images were analysed using open-access image analysis software, ImageJ (Rasband WS. U.S. National Institutes of Health, USA).

Molecular modelling of the polyamide chains. The structures and morphologies of the polymer chains with MPD and with DAHP were studied using open-access molecular modeling software ArgusLab (ArgusLab 4.0.1, Mark Thompson and Planaria Software LLC).

2.4 Desalination tests. The performance of membranes in desalination was evaluated following the method reported in a previous study [21]. Briefly, membranes were loaded in magnetically-stirred dead-end filtration cells (Sterilitech Corporation, USA) with a feed solution containing 2000 ppm NaCl. The mass of water filtered through the membrane were measured (m) over a time (t) and the water flux (F) was calculated as $F = m/(t \times A)$ where A was the effective area of the membrane used.

Conductivities of the feed (C_f) and permeate (C_p) were measured using a conductivity meter (SevenGo Pro, Mettler Toledo). The salt rejection (R) was calculated as ($1-C_p/C_f$) and C_f was calculated for each sample to correct the feed salt concentration increase due to the loss of water from the feed-side.

Intrinsic membrane resistance (R_m) was calculated from the linear regression over a range of feed pressures using an expression adapted from [15], where the pure water flux, F, is related to the transmembrane feed pressure, P, as $F=P/(\mu R_m)$ where μ is the dynamic viscosity of water.

3. Results

3.1 Synthesis of control PA TFC membranes

For the support of the PA TFC membrane, a commercial polysulfone ultrafiltration membrane was used in two different states: (i) original as received or (ii) after washing with ethanol. The original support produced PA TFC membranes with very low water flux and high salt rejection (Figure 2(a)). Increasing the MPD contact time further reduced the flux through this membrane. Typical pre-treatments such as soaking in water overnight also failed to improve the water flux to accepted levels. These observations suggested that the original polysulfone support might be more hydrophilic and thus absorbs more MPD than conventional polysulfone membranes prepared in-house [7,17]. When the support was washed in 70 % ethanol (aq) for 1 hour followed by rinsing with deionized water, the water flux through the resulting PA TFC membranes improved significantly, from a range of 0.4 – 0.8 $Lm^{-2}h^{-1}bar^{-1}$ to a range of 2.1 – 2.3 $Lm^{-2}h^{-1}bar^{-1}$. This three fold increase in permeability was achieved while keeping the same high salt rejection at 96 – 98 % (Figure 2 (a and b)).

The polysulfone supports were analysed with ATR-FTIR (Figure 2 (c)). Peaks at 1148 cm^{-1}, 1290 cm^{-1} and 1325 cm^{-1} correspond to the asymmetric vibrations of the sulfone group (-$S(O)_2$-) and the peaks at 699 cm^{-1}, 830cm^{-1}, 1583 cm^{-1} and 3094 cm^{-1} correspond to the aromatic ring

vibrations and stretching [22,23] and 1488 cm^{-1} is assigned to CH_3-C-CH_3 stretching[24] which are characteristic of polysulfone. The peak at 1024 cm^{-1} (C-O stretching) and a broad peak centered at around 3400 cm^{-1} (O-H stretching) which correspond to alcohols are visible only in the spectrum of the original support. With a few more peaks at 930 cm^{-1} and 2870 cm^{-1} corresponding to O-H bending and C-H stretching, the additional peaks in the spectrum of the original support show that there is a glycerol ($HOCH_2$-C(OH)H- H_2COH) coating on the original support. This was later confirmed by the manufacturer as the pore stabilizing agent used to protect the membrane during dry storage conditions. The ATR-FTIR results also show that the washing step has effectively removed the glycerol coating from the support surface. In fact, removal of the glycerol preservative has become a standard procedure in the membrane industry [25–28], but our work is still important for laboratory research using industrial membranes as support.

The surface roughness and static water contact angle of supports were further analyzed and summarized in Table 1. The AFM analysis shows that the surface of the as-received polysulfone support is smoother than that of the washed one while the static water contact angle is increased after the washing treatment. This is possibly due to a combined effect of removal of the hydrophilic glycerol coating and exposure of the underlying relatively rougher surface of polysulfone. This is further confirmed with SEM images which show more open pores on the surface (Figure 3 (a and b)).

The increase in the water flux through the membrane made on the washed support is therefore attributed to the removal of the glycerol coating. Glycerol is a humectant which can protect the membrane pores from collapsing under the drying conditions [26]. When used with the aqueous

phase monomer for the interfacial polymerization, glycerol acts as a wetting agent to improve the monomer attachment on to the support and avoids blocking of the support pores by the monomers [29]. However our results show that the glycerol coating made prior to the interfacial polymerization reaction affects the water flux through the resulting PA TFC membrane. This is supposed to be a combined effect of partial blocking of pores in the support with dried glycerol, and the hydrophilic nature of this coating that may result in high absorption of MPD – leading to a highly cross-linked and thick polyamide film growth on the interface as shown in the SEM images in Figure 3 (c and d). Negative effects of hydrophilic supports have also been reported previously [30]. We therefore suggest that use of clean polysulfone supports is very important for the fabrication of high-flux PA TFC membranes.

3.2 Effect of DAHP as an aqueous phase monomer: membrane performance

As shown in Figure 1, 1,3–diamino-2-hydroxypropane (DAHP) is a bifunctional aliphatic amine containing a hydroxyl group. It has a slightly lower molecular weight (90.12 g/mol) compared to MPD (108.14 g/mol). Although both the monomers are hydrophilic, DAHP has much higher affinity to water due to the presence of the polar hydroxyl group [31] and is characterized by its highly hygroscopic properties.

In PA TFC membranes, the molar ratios of $-NH_2$ to -COCl groups is an important factor determining the water flux and the salt rejection through the membrane [3,7,11] mainly due to the formation of different polymer structures at different cross-linking densities. We therefore use a previously optimized MPD: TMC ratio reported by Xie *et al.* [7] and introduce DAHP into the aqueous phase only to partially replace MPD as shown in Figure 1 and Table 2. This keeps the total $-NH_2$ concentration in the aqueous phase constant in all the experiments.

Figure 4(a) shows that when DAHP is introduced into the PA TFC membranes (PA-DAHP membranes), both the water permeability and salt rejection reach to maximum values, at 2.67 $lm^{-2}h^{-1}bar^{-1}$ (flux of 40.1 $lm^{-2}h^{-1}$) and 97% , respectively, for membranes with DAHP/MPD ratio at around 12.8%. This indicates that there is an optimum balance for the two monomers in the aqueous phase. Generally the water flux is improved from 32.7 $lm^{-2}h^{-1}$ to 40.1 $lm^{-2}h^{-1}$, by around 25%, at 12.8 % DAHP/MPD ratio for the washed support. Salt rejection remains stable at around 97 %, with the ratio of DAHP/MPD up to 20%, but significantly reduces at 30 % DAHP/MPD setting a limit for the aliphatic monomer content in the aqueous phase. The effect of DAHP was further confirmed with the PA-DAHP membranes on the original support which showed around 100 % increase in the water flux (Figure 4(b)). These results confirm that DAHP in proper combinations with MPD is useful in improving the desalination properties of PA TFC membranes.

The water flux and salt rejection through reverse osmosis membranes can be used as primary indications of the internal polymer network structure of the selective layer [21]. For PA-DAHP membrane with the DAHP/MPD ratio at 12.8 %, the high salt rejection suggests that the internal structure of the polyamide film is optimized at around this level. The intrinsic membrane resistance (R_m) is another useful parameter for understanding the structural properties [15]. R_m is calculated using the inverse of the slope of the pure water flux through the membrane as a function of the feed pressure (Figure 5(a)). The R_m reaches the lowest value of 1.05×10^{11} m^{-1} at 12.8 % and increased at 20 % and 30 % ratios (Figure 5(b)). These R_m values were calculated using a set of membranes in the lowest water flux regime for each DAHP/MPD ratio and therefore the shown R_m values would be the maximum for each monomer composition. The lowest resistance value at the 12.8 % DAHP/MPD suggests that the balance between the

polyamide layer thickness, the packing and crosslinking densities, and the active surface area would be the optimum at this point. R_m would also be affected by the mobility of internal polymer segments, the thickness and the density of the primary polyamide layer (adjacent to the support surface). The possible effects of these parameters are discussed later with analysis of the molecular structure, reaction kinetics and surface morphologies of the polyamide layer.

3.3 Effect of DAHP on the surface properties of membranes

The surface and cross-sectional SEM images of PA membranes are shown in Figure 6. The control PA membrane (MPD only) shows the characteristic ridge-and-valley structure. Generally, upon introduction of DAHP, the wide surface ridges become less frequent with the appearance of pronounced nodules formed with an average size below 100 nm.

The cross-sectional images in Figure 6 clearly show the primary and secondary layers in the polyamide film. The primary layer is the densest and has the most significant effect on the water flux [4]. The average thickness of primary layer of the control PA TFC membrane is 25.2 ± 2.1 nm. However, upon addition of DAHP, this ultra-thin layer thickness is further reduced to 20.6 ± 2.5 nm at 12.8 % DAHP/MPD which is about a 19 % reduction. At a 30 % DAHP/MPD ratio the thickness of this layer is 24.57 ± 1.65 nm. Interestingly, the water flux through the DAHP-substituted membranes inversely correlates with the thickness of the primary layer. The thickness of the secondary layer varies depending on the morphology of surface which is composed of flat ridges (ca. 160 – 190 nm in height) and nodules (ca. 75 - 90 nm in height). The incorporation of DAHP resulted in a smoother surface with the effective thickness of secondary layer reduced. The reduction in the surface roughness with the addition of the aliphatic monomer is further confirmed with AFM surface analysis (Figure 7(a)).

Figure 7 (b) shows that the static water contact angle of the unwashed PA TFC membrane is around 80˚ which is typical for aromatic PA TFC membranes [1,17,32]. The water contact angle remains almost constant with the DAHP/MPD ratio increases up to 20 % but significantly increases at 30 % DAHP/MPD ratio owing to the smoother nodular surface. The roughness has a trend towards lower values with higher DAHP whilst a notable increase in contact angle occurs at the highest DAHP. Roughness, although useful, cannot completely describe the complexity of a surface produced by interfacial polymerization. The contact angle is a function, not only of the average roughness but the lateral nature of the surface topography. This is most extremely observed in topography-driven superhydrophobicity[33–35]. Since there appears to be a transition from ridge like to nodule like surfaces, at high DAHP, this could explain the sudden increase in contact angle. However deeper studies of this transition were beyond the scope of the present paper.

3.4 Effect of DAHP on the structure of the polyamide

The polymer segment containing a DAHP unit has a more flexible backbone compared to that produced with MPD, which contains a more sterically hindering aromatic moiety. The porosity of the polymer network is believed to depend on the amount of water that diffuses with the aqueous monomer into the formed film [2,36]. Therefore, the hydrophilic DAHP can improve the internal porosity of the primary polyamide layer and the flexibility of the polymer chains is favourable to a higher water flux. However, when the local pore size exceeds the size of salt ions, the selectivity will be compromised, which might be the case at 30 % DAHP/MPD.

ATR-FTIR spectrum of the support and PA-DAHP membranes are shown in Figure 8. Since ATR-FTIR scans a depth of 1 - 2 μm on a sample, these spectra represent both the polyamide thin film and the polysulfone support. A washed support is therefore used as the blank sample. Spectra from PA-DAHP membranes show characteristic peaks at 1660 cm^{-1} (amide I band corresponding to C=O stretching), 1543 cm^{-1} (amide II band, N–H bending) and 1608 cm^{-1} (aromatic ring breathing) which are evident of the polyamide film. The broad peak between 3100-3600 cm^{-1} corresponds to O-H and N-H groups from polyamide. The peaks at 3100 - 3000 cm^{-1} and 3000 – 2900 cm^{-1} are assigned to aromatic C-H stretching and aliphatic C-H stretching, respectively, and are common to both polysulfone and polyamide [24,37]. Other common peaks arise from the polysulfone support as discussed in section 3.1. ATR-FTIR therefore confirms formation of a thin layer of polyamide on the polysulfone support at each monomer composition.

4. Discussion: mechanism of PA-DAHP membranes

This study shows that the introduction of DAHP into the polyamide film significantly alters the surface properties of the membrane as well as the structure of the polymer chains. As the fraction of DAHP in diamines increases, more nodules are formed leading to a smoother surface and reduced surface area. The thickness of the primary layer and the secondary layer are also reduced with an increase in the porosity of the polymer network.

The reduction in the thickness of the primary polyamide layer might be a result of the reduced monomer diffusion rate into the organic phase at the interface of immiscible solvents [2,4]. Since the linear monomer is more hydrophilic than its aromatic counterpart, we can assume that its diffusion rate into the organic phase is relatively slow. Slow diffusion rate of the aqueous monomers through the interface and into the organic phase results in thin polyamide films and

less hydraulic resistance [4,15,17]. This DAHP-substituted primary layer should also be more hydrophilic with more flexibility in the polymer chains and therefore more swellable than the control membrane [38] which leads to low hydraulic resistance to the permeate flux.

Aliphatic amine DAHP has a higher reactivity with TMC compared to the aromatic MPD, resulting in high condensation rates. The DAHP substituted polyamide therefore will precipitate at a more rapid rate during the interfacial polymerization resulting in a more nodular surface structure in the secondary layer. More nanosized spheres will therefore be formed at higher DAHP content. At a moderate ratio of 12.8 % DAHP/MPD, this fast precipitation might cause the ridges to become less thick and less frequent. The final result would be low surface roughness but still high surface area due to the presence of considerable amount of ridges. Previous studies also have shown that linear monomers produce membranes with less roughness [39].

In summary, the thinnest and hydrophilic polyamide dense film structure with a high surface area, enhanced polymer chain mobility and improved internal porosity is believed to create the lowest internal resistance at the 12.8 % PA-DAHP membrane for the highest flux. In contrast, lowest surface roughness and low surface area are believed to reduce the water flux at 30 % DAHP/MPD. However with interplay between the surface area, the more open internal structure and the polymer chain mobility, the water flux still remains moderate but with low rejection of salt. The significant reduction in flux and increase in internal resistance at 20 % is believed to be a result of reduced surface area while still having a less porous internal structure.

The presence of hydroxyl groups from DAHP in the polyamide films might also contributed to the enhanced water flux due to its ability to form hydrogen bonds with water molecules [31].

Intermolecular hydrogen bonds, arising from adjacent hydroxyl are known to improve the crystallinity [40]. However the hydrogen bonding does not affect the water absorption in the presence of excess water since water absorbed into the polymer breaks hydrogen bonding between hydroxyl groups [41]. On the other hand, hydroxyl groups can react with TMC to form network structure (e.g. ether linkages) which also might be responsible for the reduced water flux at high DAHP ratios.

5. Conclusions

We demonstrate that the water flux through a PA TFC membrane can be improved by incorporating DAHP, a linear hydrophilic amine, in proper combination with the conventional aqueous phase monomer MPD. The surface morphology, thickness of the polyamide film and the structure of the polymer network are significantly changed with introduction of DAHP and as a result the surface roughness is reduced. The change in thickness inversely correlates with the improved water flux and is believed to be an effect of the slow diffusion rate of DAHP to the organic phase.

The reduced thickness, hydrophilicity and polymer chain mobility of the polyamide selective layer renders the high water flux for the PA-DAHP membrane while the reduced surface area due to loss of ridges negatively affects the water flux. A balance between these two set of parameters results in the minimum internal resistance for the highest water flux at DAHP/MPD ratio of 12.8%. The reduced surface roughness will also be beneficial as it is always associated with less surface colloidal fouling [42–44].

This work shows that selection of monomers with proper degree of hydrophilicity, diffusion rate as well as the structure can significantly alter the surface properties and the internal structure of polyamide thin films. Also the understanding of the mechanism of the formation of the polyamide layer would be useful to synthesize highly optimized selective layers for better performance.

We also show that clean coating-free support is important for fabrication of high flux PA TFC membranes. Washing with ethanol effectively removed the surface glycerol coating on the commercial support and resulted in a dramatic improvement in the water flux from the resulting

PA TFC membrane. This illustrates the strong relationship between the surface properties of the support membrane and the desalination performance of the PA TFC membranes.

Acknowledgements:

We would like to thank EPSRC grant, Schlumberger Faculty for the Future (FFTF) foundation and the Qatar National Research Fund for the research financial support. Robert Cornell from Department of Materials Science is acknowledged for his support with ATR-FTIR.

References:

1. Lau, W. J., Ismail, A. F., Misdan, N. & Kassim, M. A. A recent progress in thin film composite membrane: A review. *Desalination* **287,** 190–199 (2012).

2. Janssen, L. & Nijenhuis, K. Te. Encapsulation by interfacial polycondensation. I. The capsule production and a model for wall growth. *J. Memb. Sci.* **65,** 59–68 (1992).

3. Song, Y., Sun, P., Henry, L. & Sun, B. Mechanisms of structure and performance controlled thin film composite membrane formation via interfacial polymerization process. *J. Memb. Sci.* **251,** 67–79 (2005).

4. Jin, Y. & Su, Z. Effects of polymerization conditions on hydrophilic groups in aromatic polyamide thin films. *J. Memb. Sci.* **330,** 175–179 (2009).

5. Chai, G.-Y. & Krantz, W. B. Formation and characterization of polyamide membranes via interfacial polymerization. *J. Memb. Sci.* **93,** 175–192 (1994).

6. Ghosh, A. K., Jeong, B. H., Huang, X. & Hoek, E. M. V. Impacts of reaction and curing conditions on polyamide composite reverse osmosis membrane properties. *J. Memb. Sci.* **311,** 34–45 (2008).

7. Xie, W. *et al.* Polyamide interfacial composite membranes prepared from m-phenylene diamine, trimesoyl chloride and a new disulfonated diamine. *J. Memb. Sci.* **403-404,** 152–161 (2012).

8. Kwak, S. Y., Jung, S. G., Yoon, Y. S. & Ihm, D. W. Details of surface features in aromatic polyamide reverse osmosis membranes characterized by scanning electron and atomic force microscopy. *J. Polym. Sci. B Polym. Phys.* **37,** 1429–1440 (1999).

9. Zhao, L., Chang, P. C.-Y. & Ho, W. S. W. High-flux reverse osmosis membranes incorporated with hydrophilic additives for brackish water desalination. *Desalination* **308,** 225–232 (2013).

10. Roh, I. J. & Khare, V. P. Investigation of the specific role of chemical structure on the material and permeation properties of ultrathin aromatic polyamides. *J. Mater. Chem* **12,** 2334–2338 (2002).

11. Rao, P. A., Joshi, S. V., Trivedi, J. J., Devmurari, C. V. & Shah, V. J. Structure–performance correlation of polyamide thin film composite membranes: effect of coating conditions on film formation. *J. Memb. Sci.* **211,** 13–24 (2003).

12. Tang, C. Y., Kwon, Y.-N. & Leckie, J. O. Effect of membrane chemistry and coating layer on physiochemical properties of thin film composite polyamide RO and NF membranes. *Desalination* **242,** 168–182 (2009).

13. Guillen, G. R., Hoek, E. M. V., Lind, M. L. & Wong, M. C. Forward osmosis membrane with blended polymeric support. Patent: WO2012149141 A1 (2012).

14. Tang, B., Zou, C. & Wu, P. Study on a novel polyester composite nanofiltration membrane by interfacial polymerization. II. The role of lithium bromide in the performance and formation of composite membrane. *J. Memb. Sci.* **365,** 276–285 (2010).

15. Baroña, G. N. B., Lim, J. & Jung, B. High performance thin film composite polyamide reverse osmosis membrane prepared via m-phenylenediamine and 2,2′-benzidinedisulfonic acid. *Desalination* **291,** 69–77 (2012).

16. Yong, Z., Sanchuan, Y., Meihong, L. & Congjie, G. Polyamide thin film composite membrane prepared from m-phenylenediamine and m-phenylenediamine-5-sulfonic acid. *J. Memb. Sci.* **270,** 162–168 (2006).

17. Wang, H., Li, L., Zhang, X. & Zhang, S. Polyamide thin-film composite membranes prepared from a novel triamine 3,5-diamino-N-(4-aminophenyl)-benzamide monomer and m-phenylenediamine. *J. Memb. Sci.* **353,** 78–84 (2010).

18. Li, L., Zhang, S., Zhang, X. & Zheng, G. Polyamide thin film composite membranes prepared from 3,4′,5-biphenyl triacyl chloride, 3,3′,5,5′-biphenyl tetraacyl chloride and m-phenylenediamine. *J. Memb. Sci.* **289,** 258–267 (2007).

19. Fibiger, R. F. *et al.* Novel polyamide reverse osmosis membranes. Patent: US 4769148 (1988).

20. Jeong, B. H. *et al.* Interfacial polymerization of thin film nanocomposites: A new concept for reverse osmosis membranes. *J. Memb. Sci.* **294,** 1–7 (2007).

21. Perera, D. H. N. *et al.* Room-temperature development of thin film composite reverse osmosis membranes from cellulose acetate with antibacterial properties. *J. Memb. Sci.* **453,** 212–220 (2014).

22. Rupiasih, N. N., Suyanto, H., Sumadiyasa, M. & Wendri, N. Study of Effects of Low Doses UV Radiation on Microporous Polysulfone Membranes in Sterilization Process. *Open J. Org. Polym. Mater.* **3,** 12–18 (2013).

23. Junaidi, M. U. M., Leo, C. P., Ahmad, a. L., Kamal, S. N. M. & Chew, T. L. Carbon dioxide separation using asymmetric polysulfone mixed matrix membranes incorporated with SAPO-34 zeolite. *Fuel Process. Technol.* **118,** 125–132 (2014).

24. Singh, P. S. *et al.* Probing the structural variations of thin film composite RO membranes obtained by coating polyamide over polysulfone membranes of different pore dimensions. *J. Memb. Sci.* **278,** 19–25 (2006).

25. Bohonak, D. M. & Zydney, A. L. Compaction and permeability effects with virus filtration membranes. *J. Memb. Sci.* **254,** 71–79 (2005).

26. Shukla, R. & Cheryan, M. Performance of ultrafiltration membranes in ethanol – water solutions : effect of membrane conditioning. *J. Memb. Sci.* **198,** 75–85 (2002).

27. Jones, S. a., Bird, M. R. & Pihlajamäki, A. An experimental investigation into the pre-treatment of synthetic membranes using sodium hydroxide solutions. *J. Food Eng.* **105,** 128–137 (2011).

28. Wright, S., Pellegrino, J. & Amy, G. Humectant release from membrane materials. *J. Memb. Sci.* **246,** 227–234 (2005).

29. Kuehne, M. A., Song, R. Q., Li, N. N. & Petersen, R. J. Flux enhancement in TFC RO membranes. *Environ. Prog.* **20,** 23–26 (2001).

30. Ghosh, A. K. & Hoek, E. M. V. Impacts of support membrane structure and chemistry on polyamide–polysulfone interfacial composite membranes. *J. Memb. Sci.* **336,** 140–148 (2009).

31. Thijs, H. M. . *et al.* Water uptake of hydrophilic polymers determined by a thermal gravimetric analyzer with a controlled humidity chamber. *J. Mater. Chem.* **17,** 4864–4871 (2007).

32. Lind, M. L., Suk, D. E., Nguyen, T.-V. & Hoek, E. M. V. Tailoring the structure of thin film nanocomposite membranes to achieve seawater RO membrane performance. *Environ. Sci. Technol.* **44,** 8230–8235 (2010).

33. Chu, Z. & Seeger, S. Superamphiphobic surfaces. *Chem. Soc. Rev.* **43,** 2784–2798 (2014).

34. Ganesh, V. A., Raut, H. K., Nair, A. S. & Ramakrishna, S. A review on self-cleaning coatings. *J. Mater. Chem.* **21,** 16304 (2011).

35. Thorvaldsson, A. *et al.* Superhydrophobic behaviour of plasma modified electrospun cellulose nanofiber-coated microfibers. *Cellulose* **19,** 1743–1748 (2012).

36. Ji, J., Dickson, J. M., Childs, R. F. & McCarry, B. E. Mathematical Model for the Formation of Thin-Film Composite Membranes by Interfacial Polymerization: Porous and Dense Films. *Macromolecules* **33,** 624–633 (2000).

37. Tang, C. Y., Kwon, Y. & Leckie, J. O. Probing the nano- and micro-scales of reverse osmosis membranes — A comprehensive characterization of physiochemical properties of uncoated and coated membranes by XPS , TEM , ATR-FTIR , and streaming potential measurements. *J. Membr. Sci.* **287,** 146–156 (2007).

38. Chan, E. P., Young, A. P., Lee, J. & Stafford, C. M. Swelling of Ultrathin Molecular Layer-by-Layer Polyamide Water Desalination Membranes. *J. Polym. Sci. Part B Polym. Phys.* **51,** 1647–1655 (2013).

39. Huang, Y. H. *et al.* Investigation of fine-structure of polyamide thin-film composite membrane under swelling effect by positron annihilation lifetime spectroscopy and molecular dynamics simulation. *J. Memb. Sci.* **417-418,** 201–209 (2012).

40. Hodge, R. M. Water absorption and states of water in semicrystalline poly(vinyl alcohol) films. *Polymer (Guildf).* **37,** 1371–1376 (1996).

41. Hatakeyama, H. & Hatakeyama, T. Interaction between water and hydrophilic polymers l. *Thermochim. Acta* **308,** 3–22 (1998).

42. Elimelech, M., Zhu, X., Childress, A. E. & Hong, S. Role of membrane surface morphology in colloidal fouling of cellulose acetate and composite aromatic polyamide reverse osmosis membranes. *J. Membr. Sci.* **127,** 101–109 (1997).

43. Hoek, E. M. V, Bhattacharjee, S. & Elimelech, M. Effect of Membrane Surface Roughness on Colloid-Membrane DLVO Interactions. *Langmuir* **19,** 4836–4847 (2003).

44. Zhu, X. H. & Elimelech, M. Colloidal fouling of reverse osmosis membranes: Measurements and fouling mechanisms. *Environ. Sci. Technol.* **31,** 3654–3662 (1997).

Schemes, Tables and Figures

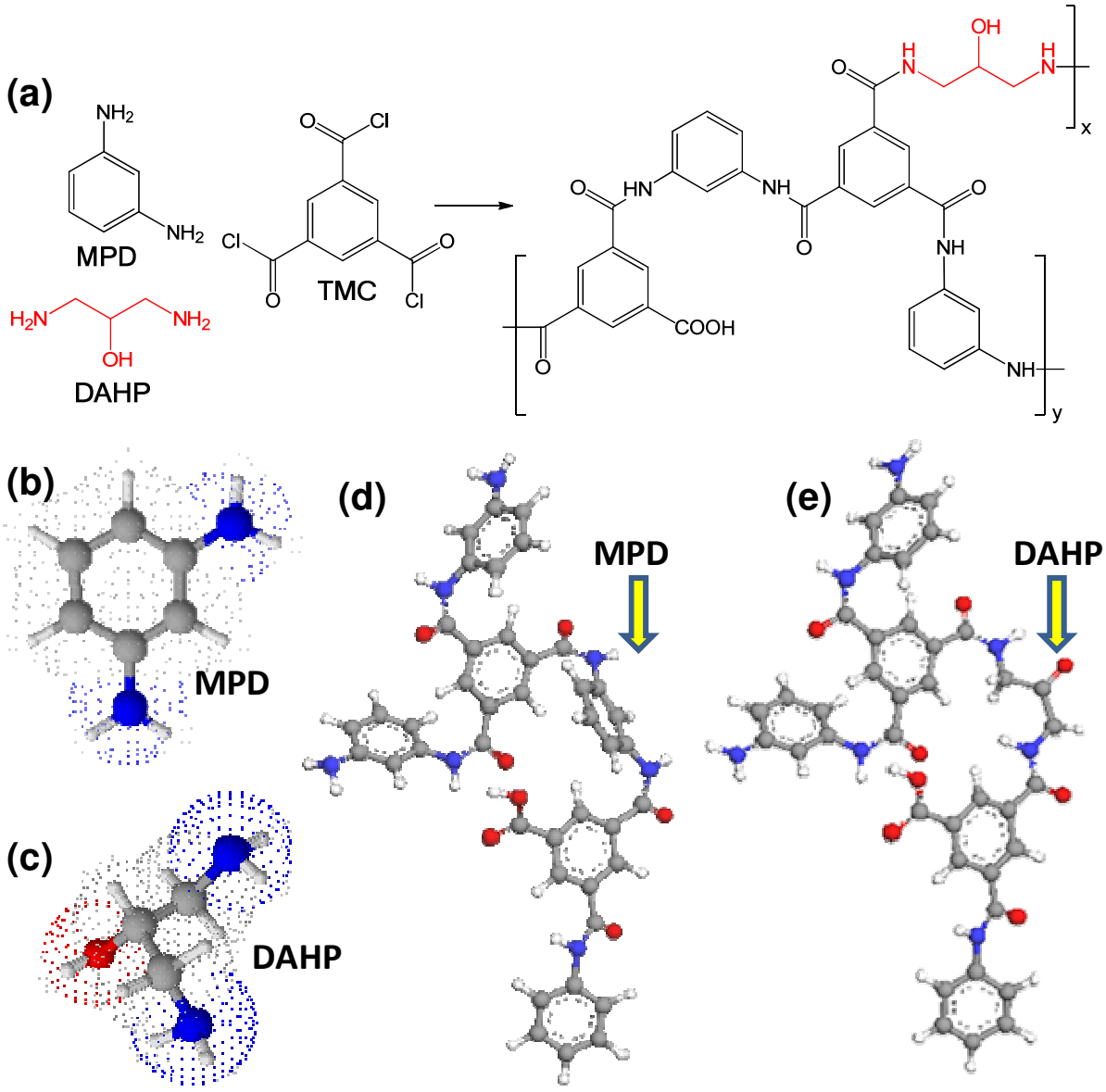

Figure 1. Synthesis of polyamide. (a) Synthesis of polyamide network from interfacial polymerization of m-phenylenediamine (MPD), 1,3–diamino-2-hydroxypropane (DAHP) and 1,3,5-benzenetricarbonyl trichloride (TMC). (b) Charge density map of MPD and DAHP. (c) Visualization of segments of DAHP-substituted polyamide network (carbon - grey, nitrogen – blue, oxygen – red, and hydrogen – white).

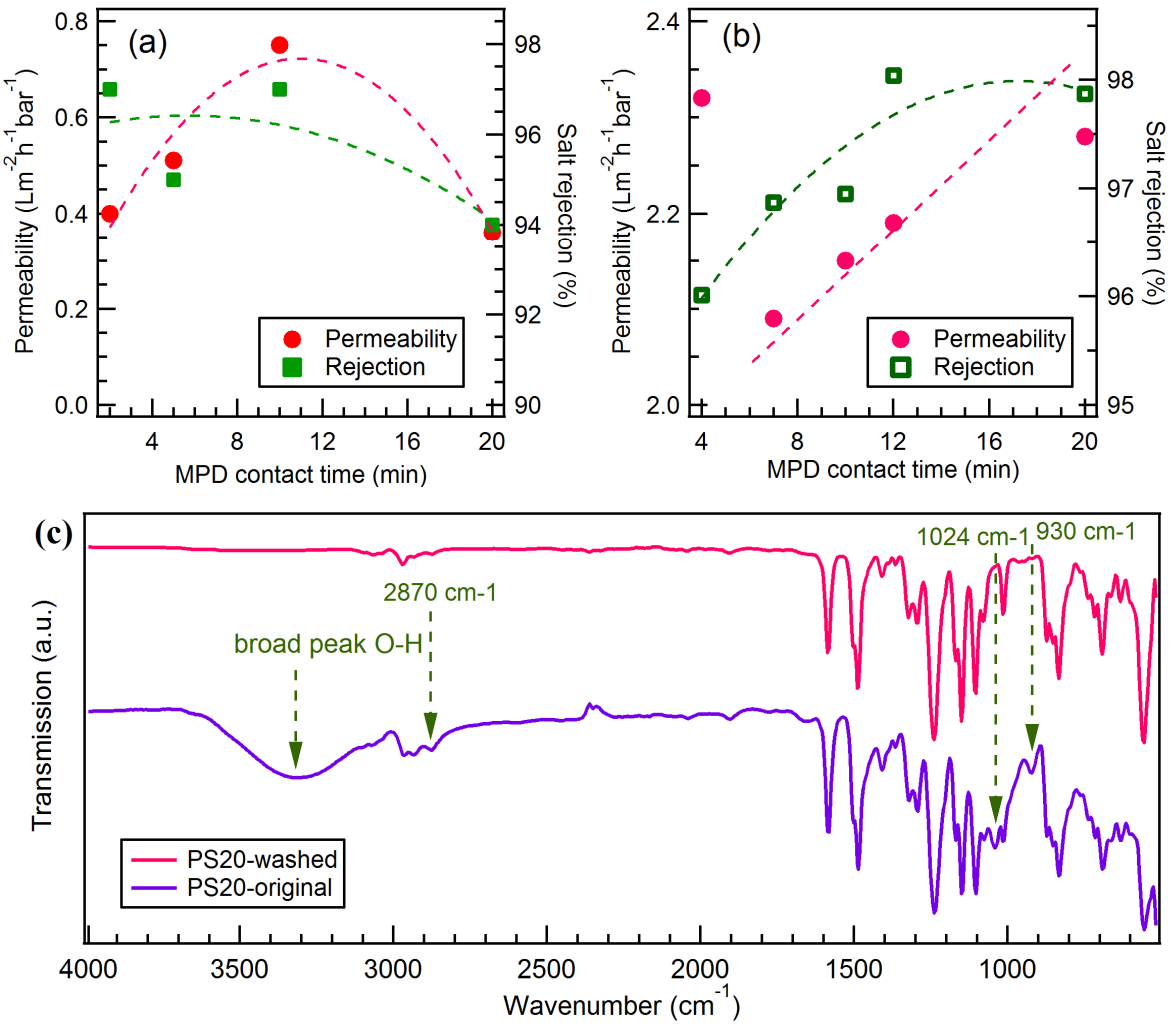

Figure 2: Desalination performance of PA TFC membranes made on the (a) original polysulfone support and on (b) washed polysullfone support. (c) ATR-FTIR spectra of the surfaces of original and washed polysulfone membranes. Membranes were tested at a feed pressure of 15 bar.

Support membrane	Surface Roughness		Water contact angle (degrees)
	R_a	R_{rms}	
Original	3.35 nm	4.32 nm	47.7 ± 12.2
Washed	10.3 nm	20.4 nm	56.8 ± 6.7

Table 1: Surface properties of polysulfone support before and after washing. R_a = average roughness, R_{rms} = root-mean-square roughness over a surface area of 5 x 5 μm.

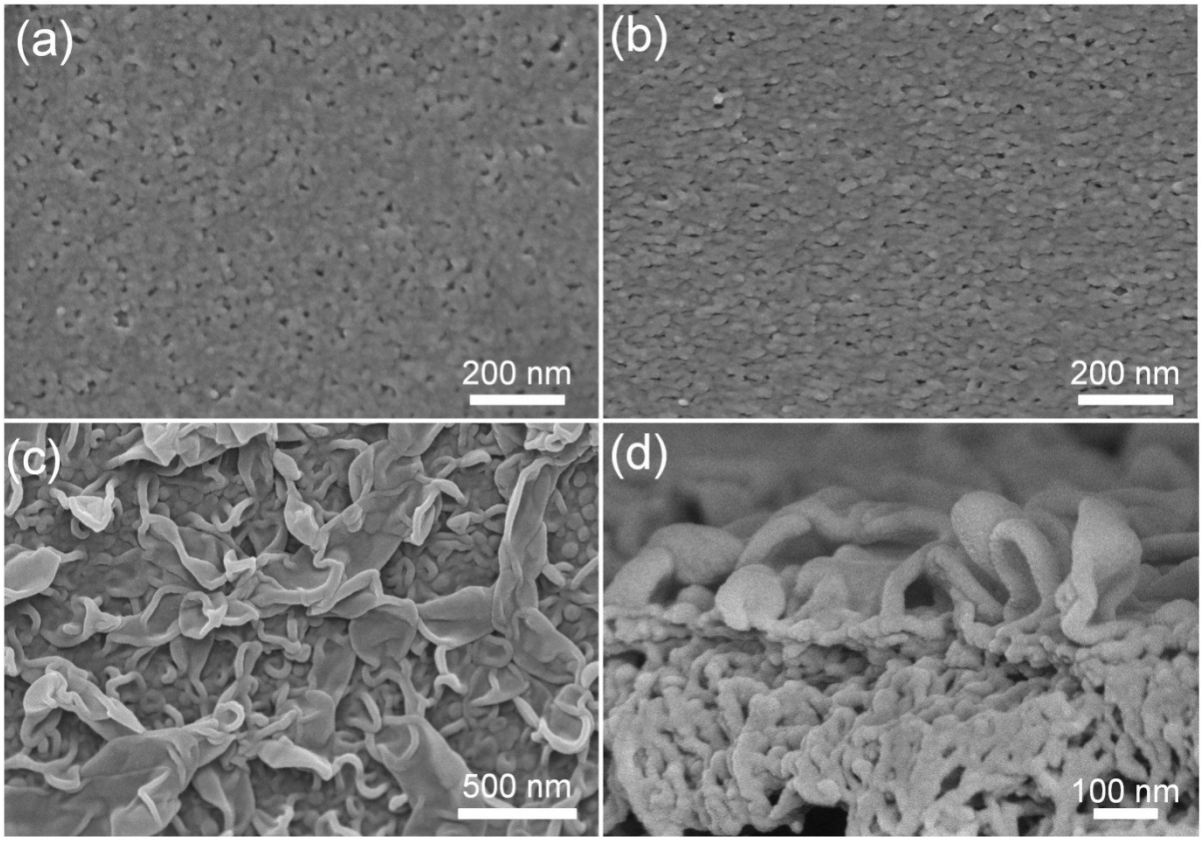

Figure 3: SEM images of surfaces of (a) original and (b) washed polysulfone support. (c) Surface and (d) cross-sectional SEM images of polyamide TFC membranes synthesized from interfacial polymerization on unwashed polysulfone support.

Aqueous phase				Organic phase
DAHP / MPD (w/w %)	MPD (w/v) %	DAHP (w/v) %	Total [–NH_2] (mol/100ml)	TMC in dodecane
0.0	1.5	0.0000	0.0277	0.05 (w/v) % (or [-COCl] = 0.000565 mol/100ml)
6.0	1.4	0.0840	0.0277	
12.8	1.3	0.1167	0.0277	
20.0	1.2	0.2500	0.0277	
30.0	1.1	0.3340	0.0277	

Table 2: The composition of the monomers in the aqueous phase and the organic phase for the PA-DAHP TFC membranes

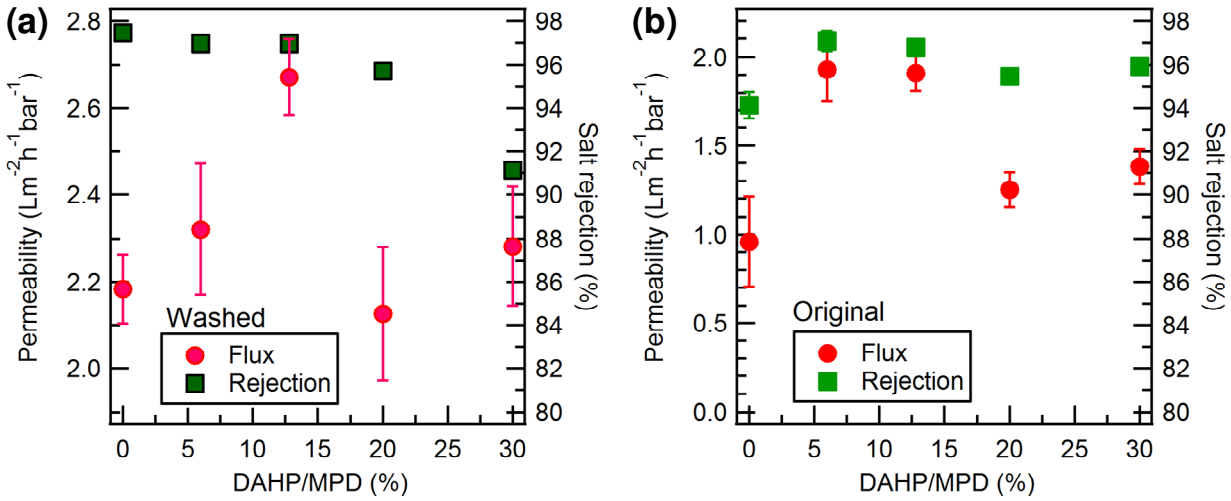

Figure 4: The permeate flux and salt rejection of PA-DAHP TFC membranes (a) on the washed support and (b) on the original support as a function of DAHP/MPD ratio in the aqueous phase. All the membranes were tested at 15 bar and with 2000 ppm NaCl as the feed. The error bars show the standard error of the mean (n≥ 3).

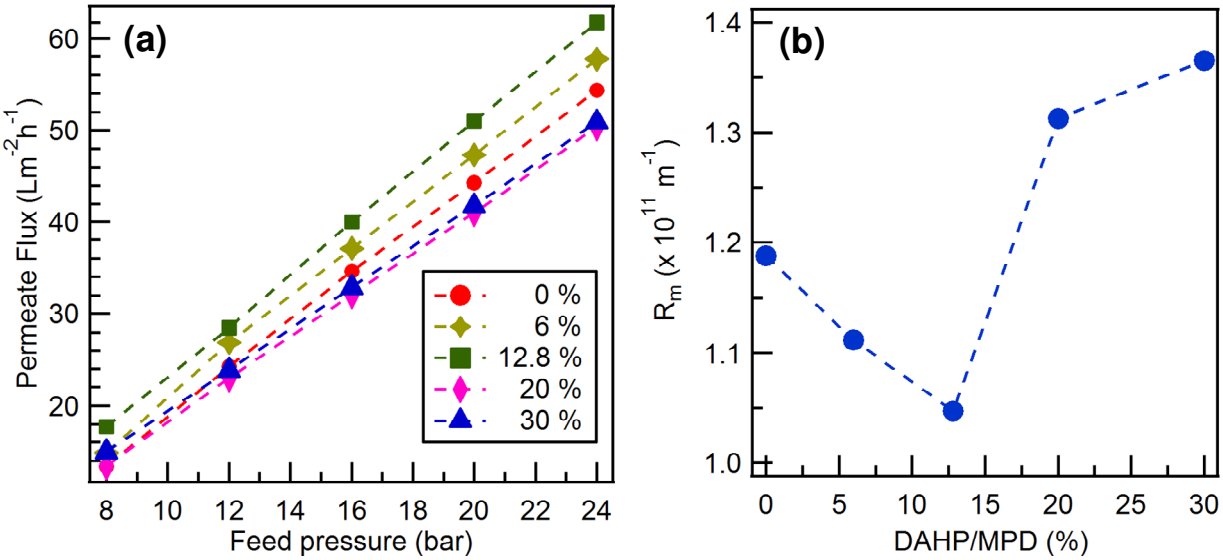

Figure 5: (a) The pure water flux as a function of feed pressure and (b) the intrinsic resistance of a set of membranes representing the low flux regime in Figure 4 (a). The fit lines are for visual purpose only.

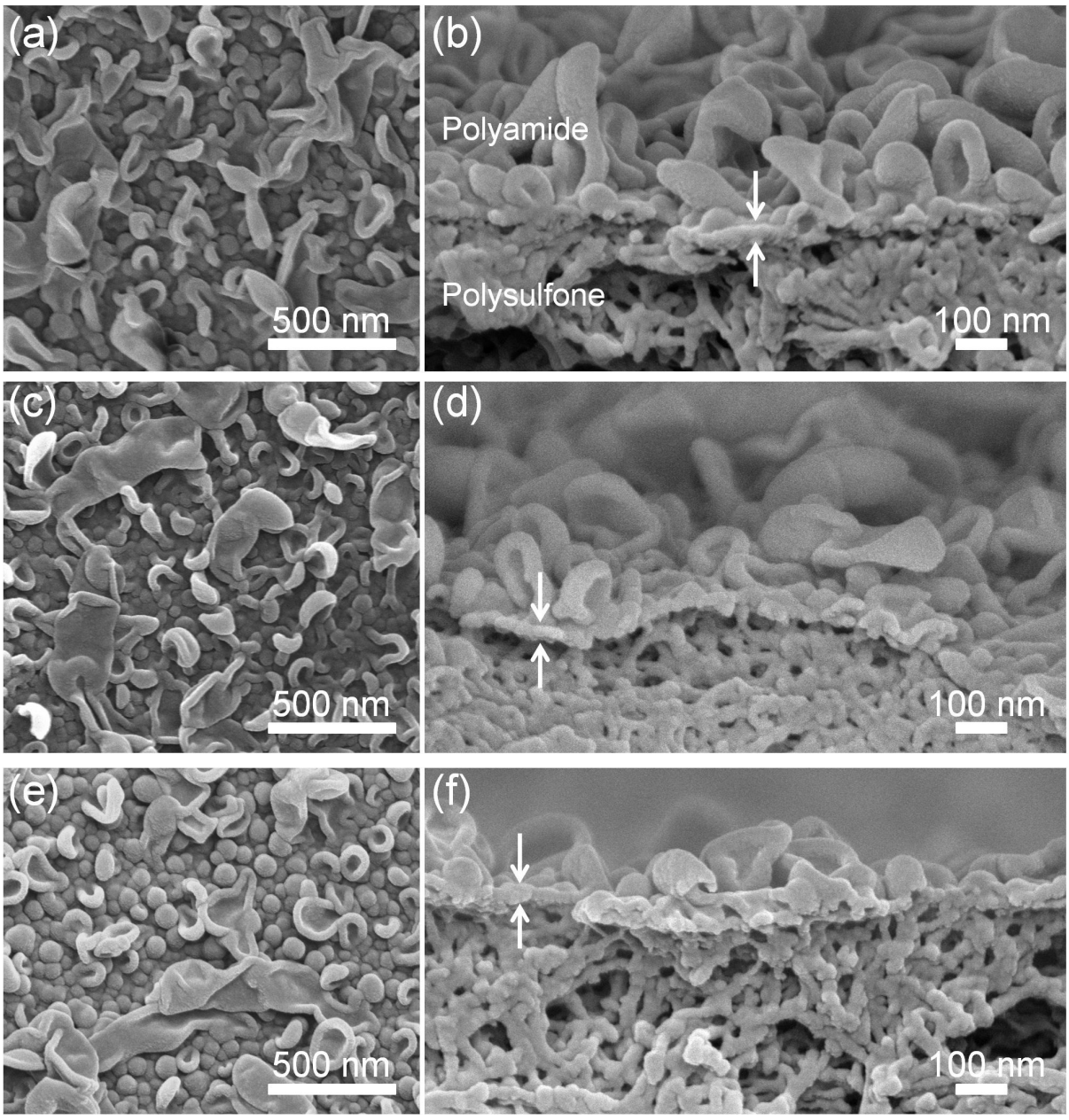

Figure 6: SEM images of polyamide TFC membranes on washed polysulfone supports. Polyamide membranes were synthesized from interfacial polymerization of TMC with pure MPD (a-b), a mixture MPD and DAHP (12.8 wt%) (c-d), and a mixture of MPD and DAHP (30 wt%) (e-f). Arrows indicate the thickness of the primary layer. (a,c,e) Surface; (b,d,f) Cross-sections.

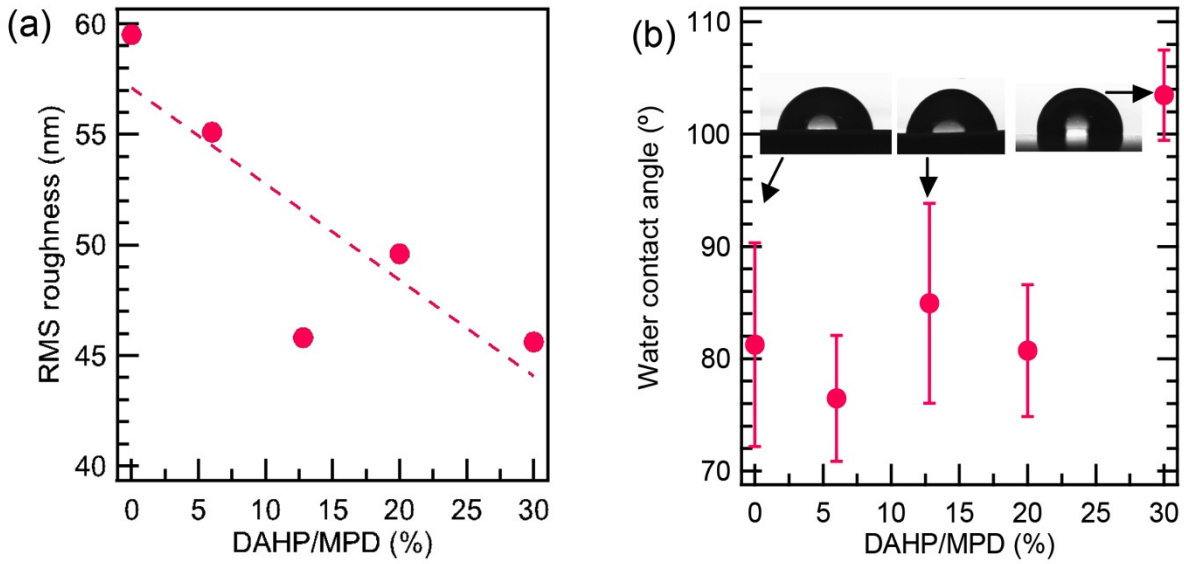

Figure 7: Changes in surface properties of PA TFC membrane with partial replacement of MPD with DAHP: (a) surface roughness and (b) static water contact angle. Fit line is for visual guidance only.

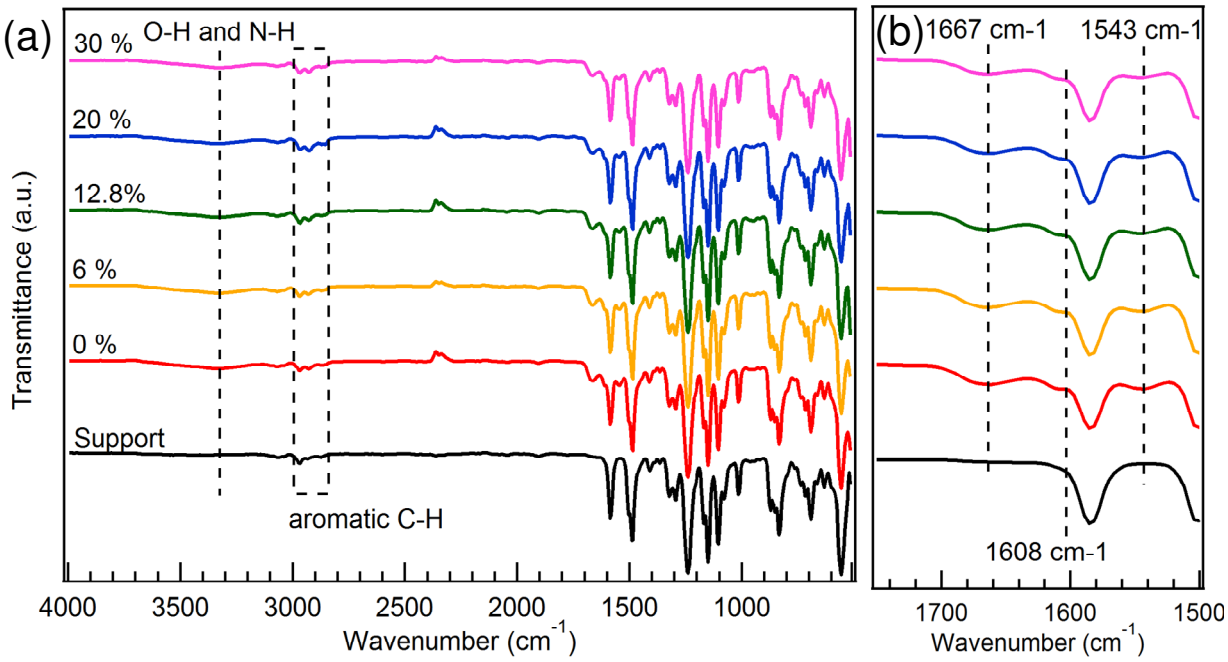

Figure 8: (a) ATR-FTIR spectra of PA-DAHP TFC membranes on washed support and (b) expanded spectra showing the functional group region from 1800 cm^{-1} – 1500 cm^{-1} .

For Table of Contents Use Only

Table of Contents Graphic:

Regulating the aqueous phase monomer balance for flux improvement in polyamide thin film composite membranes D.H.N. Perera, Q. Song, H.A.M. Qiblawey and E. Sivaniah	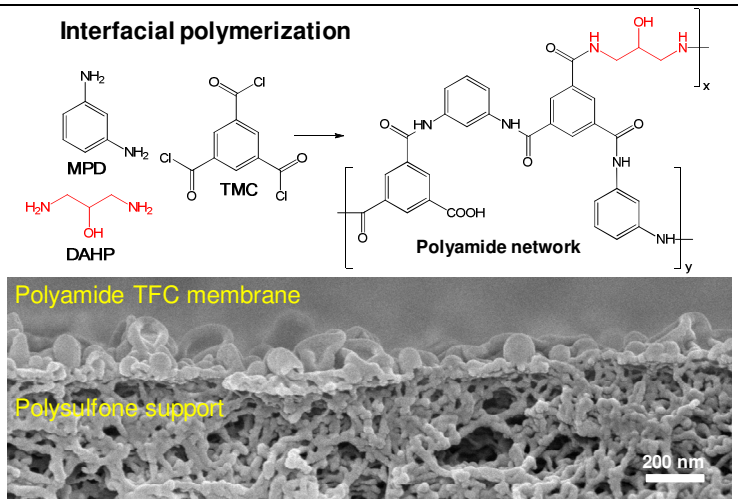

For Table of Contents Use Only

Table of Contents Graphic:

Regulating the aqueous phase monomer balance for flux improvement in polyamide thin film composite membranes D.H.N. Perera, Q. Song, H.A.M. Qiblawey and E. Sivaniah